PLOS ONE

RESEARCH ARTICLE

A Semi-Physiologically Based Pharmacokinetic Pharmacodynamic Model for Glycyrrhizin-Induced Pseudoaldosteronism and Prediction of the Dose Limit Causing Hypokalemia in a Virtual Elderly Population

Ruijuan Xu, Xiaoquan Liu*, Jin Yang*

Key Laboratory of Drug Metabolism and Pharmacokinetics, China Pharmaceutical University, Nanjing, China

*yjcpu@yahoo.com (JY); lxq_cpu@yahoo.com.cn (XL)

CrossMark
click for updates

OPEN ACCESS

Citation: Xu R, Liu X, Yang J (2014) A Semi-Physiologically Based Pharmacokinetic Pharmacodynamic Model for Glycyrrhizin-Induced Pseudoaldosteronism and Prediction of the Dose Limit Causing Hypokalemia in a Virtual Elderly Population. PLoS ONE 9(12): e114049. doi:10.1371/journal.pone.0114049

Editor: Sebastien Fuchs, Cedars-Sinai Medical Center, United States of America

Received: April 1, 2014

Accepted: October 16, 2014

Published: December 2, 2014

Copyright: © 2014 Xu et al. This is an open-access article distributed under the terms of the Creative Commons Attribution License, which permits unrestricted use, distribution, and reproduction in any medium, provided the original author and source are credited.

Data Availability: The authors confirm that all data underlying the findings are fully available without restriction. All relevant data are within the paper and its Supporting Information files.

Funding: Funding provided by Chinese foundation for hepatitis prevention and control——TianQing liver disease research fund subject TQGB2011017 URLs: http://www.cfhpc.org/. The funders had no role in study design, data collection and analysis, decision to publish, or preparation of the manuscript.

Competing Interests: The authors have declared that no competing interests exist.

Abstract

Glycyrrhizin (GL) is a widely used food additive which can cause severe pseudoaldosteronism at high doses or after a long period of consumption. The aim of the present study was to develop a physiologically based pharmacokinetic (PBPK) pharmacodynamic (PD) model for GL-induced pseudoaldosteronism to improve the safe use of GL. Since the major metabolite of GL, glycyrrhetic acid (GA), is largely responsible for pseudoaldosteronism via inhibition of the kidney enzyme 11β-hydroxysteroiddehydrogenase 2 (11β-HSD 2), a semi-PBPK model was first developed in rat to predict the systemic pharmacokinetics of and the kidney exposure to GA. A human PBPK model was then developed using parameters either from the rat model or from in vitro studies in combination with essential scaling factors. Kidney exposure to GA was further linked to an I_{max} model in the 11β-HSD 2 module of the PD model to predict the urinary excretion of cortisol and cortisone. Subsequently, activation of the mineralocorticoid receptor in the renin-angiotensin-aldosterone-electrolyte system was associated with an increased cortisol level. Experimental data for various scenarios were used to optimize and validate the model which was finally able to predict the plasma levels of angiotensin II, aldosterone, potassium and sodium. The Monte Carlo method was applied to predict the probability distribution of the individual dose limits of GL causing pseudoaldosteronism in the elderly according to the distribution of sensitivity factors using serum potassium as an indicator. The critical value of the dose limit was found to be 101 mg with a probability of 3.07%.

Introduction

Glycyrrhizin (GL), one of the major components in licorice root, is widely used as a sweetener in food products and chewing tobacco. In addition, GL is of clinical importance as an antiinflammatory and hepatoprotective agent in the treatment of dermatitis, gastritis, hepatitis and other conditions [1]. However, several studies have reported that excessive or long-term consumption of GL can induce adverse effects such as hypertension, hypokalemia and sodium retention, all of which are symptoms of pseudoaldosteronism. In serious cases, the outcome can be death [2].

The mechanism of this pseudoaldosteronism seems to be clear [3]. Glycyrrhetic acid (GA), the main metabolite of GL, has been verified to be the major substance leading to pseudoaldosteronism. GA is a potent inhibitor of 11β-hydroxysteroiddehydrogenase 2 (11β-HSD 2), the enzyme that converts cortisol to cortisone in the kidney. This inhibition leads to an increase in cortisol levels as well as in the cortisol:cortisone ratio in plasma and urine and, as cortisol and aldosterone have the same affinity for the mineralocorticoid receptor (MR) [4], to increased stimulation of the MR leading to increased electrolyte levels and the symptoms of pseudoaldosteronism.

The metabolism of GL depends on its route of administration [5]. GL administered by the intravenous (i.v.) route is partially hydrolyzed in the liver by lysosomal β-D-glucuronidase to 3-monoglucuronyl-glycyrrhretinic acid (3MGA). GL and 3MGA can then be excreted into the bile via canalicular transporters and finally reach the intestinal lumen. There GL and 3MGA are metabolized by the intestinal microbiota to GA, which then undergoes enterohepatic recycling. When GL is administered by the oral route (p.o.), the intestinal microbiota bring about its hydrolysis to GA which again undergoes enterohepatic recycling.

In assessing the risk of a food additive, the traditional method of measuring the acceptable daily intake, following the rule of 'dividing by ten', is arbitrary and provides an inaccurate estimation. It is a feasible and recommended method when the mechanism of action for the compound in question is not quite clear. However, a large number of in vivo and in vitro studies have recently reported the mechanisms of GL pharmacokinetics and GL-induced pseudoaldosteronism. We therefore attempted to use the method of mechanism-based modeling to make the risk control process more accurate and reasonable. Moreover, according to the opinions of the Scientific Committee on Food (SCF) [6] and the Dutch Nutrition Information Bureau (DNIB) [7], the upper safe limits for regular ingestion of GL are 100 mg/day and 200 mg/day respectively. However, because human toxicity studies remain incomplete, these upper limits may actually be too high to ensure sufficient protection to some subgroups. Consequently, modeling and simulation of scenarios difficult to undertake in clinical studies are needed to provide more accurate predictions of the dose limit in various populations. In addition, since the kidney is the target tissue of GA in GL-induced pseudoaldosteronism, determination of kidney exposure to GA in such populations is important to predict the likelihood of adverse effects of GL.

Physiologically-based pharmacokinetic (PBPK) modeling is now an established technique for estimating the absorption, distribution, metabolism and excretion of a drug and, in combination with pharmacodynamic (PD) modeling, predicting its pharmacological and/or adverse effects. Ploeger and colleagues developed a PBPK/PD model of GL in rat and human [8, 9, 10] and successfully predicted GL and GA plasma concentrations and the urinary cortisol:cortisone ratio in human. However, in the Ploeger model, the urinary cortisol:cortisone ratio did not indicate whether an adverse event had actually occurred. We therefore recognized the need to include in the model the clinical indicators of pseudoaldosteronism (e.g. serum potassium and sodium levels) and the kidney exposure to GA in order to better predict the adverse effects of GL. Moreover, once the MR is over-stimulated, the renin-angiotensin-aldosterone system (RAAS) is inhibited as a compensatory effect meaning RAAS also plays an important role in changing the levels of body fluids and electrolytes when GL is ingested.

In the present study, we first developed a semi-PBPK model for GL and GA in rat and then, based on parameters in the rat model and species scaling, developed a human PBPK model in which kidney exposure to GA was further combined with a biological system-PD model to produce a PBPK/PD model capable of predicting the indicators of GL-induced pseudoaldosteronism in human.

Materials and Methods

Experimental studies

During the modeling process, optimization and validation were conducted step by step using in vivo experimental datasets largely based on the literature. Moreover, in order to ask the validation more robust, we found it necessary to have data relating to the PK of GA and its kidney distribution after p.o. administration of GL. Two separate studies as follows were first conducted to provide a validation dataset for the rat PBPK model.

Materials

GL and GA (purity >98%) were obtained from Chia-tai Tianqing Pharmaceutical Co, Nanjing, China. Diclofenac for use as internal standard (IS) was purchased from Nanjing Chemical Reagent Co Ltd., Nanjing, China. All other chemicals were of analytical grade and used as received. Ultrapure water was used in all studies.

Male Sprague-Dawley rats (weight 220–250 g) were obtained from B&K Universal Group Ltd., Shanghai, China. The rats were housed under a 12 h light/dark cycle with free access to commercial rat chow and water. All animals were fasted overnight with free access to water before an experiment. All animal experiments were approved by the Animal Ethics Committee of China Pharmaceutical University and performed under a license granted by the Jiangsu Science and Technology Office (China). All efforts were made to minimize suffering.

Pharmacokinetics of GA after p.o. administration of GL

GL was dissolved in ultrapure water and administered p.o. to 5 rats at 100 mg/kg. Blood samples (0.2 ml) were collected at the following time points: 0.5, 1, 2, 4, 6, 8, 12, 24 h after the dose. Samples were stored at −20℃ pending analysis.

Kidney distribution of GA after p.o. administration of GL

A group of 12 rats received a p.o. dose of GL at 200 mg/kg. After 9, 16 and 22 h, 4 animals were sacrificed at each time point by femoral artery exsanguination and blood and kidneys harvested. Each tissue was homogenized with an equal volume of cold saline after which samples were stored at −20℃ pending analysis.

Analysis of GA in rat plasma and kidney

GA concentrations in the above samples were analyzed according to a previously developed method [11]. 90 μl plasma or tissue homogenate was taken into an Eppendorf tube, and added to 10 ml diclofenac (internal standard, 1 μg/ml) and 200 ml acetonitrile. The tube was vortex mixed and then centrifuged at 13000 × g for 10 min. The supernatant was transferred to another clean Eppendorf tube and centrifuged at 13000 × g for 10 min. An aliquot (5 μl) of supernatant was injected directly onto the HPLC column. And the analysis was carried out by LC-MS using an LC-MS 2010 system (Shimadzu, Kyoto Prefecture, Japan) comprising 2 LC-20AD pumps, a CBM-20A system controller, a CTO-20A column oven set at 40℃, a SIL-20AC autosampler set to inject 5 μL and a single quadrupole mass spectrometer equipped with an electrospray ionization (ESI) interface operated in the negative ionization mode. Separation was carried out on an Agilent Microsorb 100–5 C18 column (150 × 2.0 mm) using gradient elution with 0.1% acetic acid-10 mM ammonium acetate in water as mobile phase A and acetonitrile as mobile phase B at a fl ow rate of 0.2 mL/min. The gradient (min, %B) was as follows: 0–0.5, 20; 0.5–2.5, 40; 2.5–6.5, 90; 6.5–10.0, 20. Elution in the period 2.5–7.0 min was delivered into the mass analyzer. Detection was by selected ion monitoring (SIM) of ions with 469.3 for GA and 294.1 for diclofenac (internal standard IS). Optimum MS parameters were: Capillary voltage − 1.5 kV; nebulizer nitrogen flow rate 1.5 L/min; drying gas temperature 280℃; block temperature 220℃.

Model building workflow

Following the proposed workflow shown in Figure 1, a PBPK/PD model for GL-induced pseudoaldosteronism was developed and used to predict the dose limit of GL producing pseudoaldosteronism in a virtual population. In brief, the rat PBPK model was first developed. Physicochemical parameters, absorption, distribution, metabolism and elimination (ADME) data, and physiological parameters were collected from the literature and used as initial input parameters of the model. After that, in vivo data sets were used: some to optimize, some to validate the model. If the model adequately reflected the observed data, the modeling process was continued; if not, the process would revert to the first step (see flowchart in figure 1). Based on the structure and parameters of rat PBPK model and also on

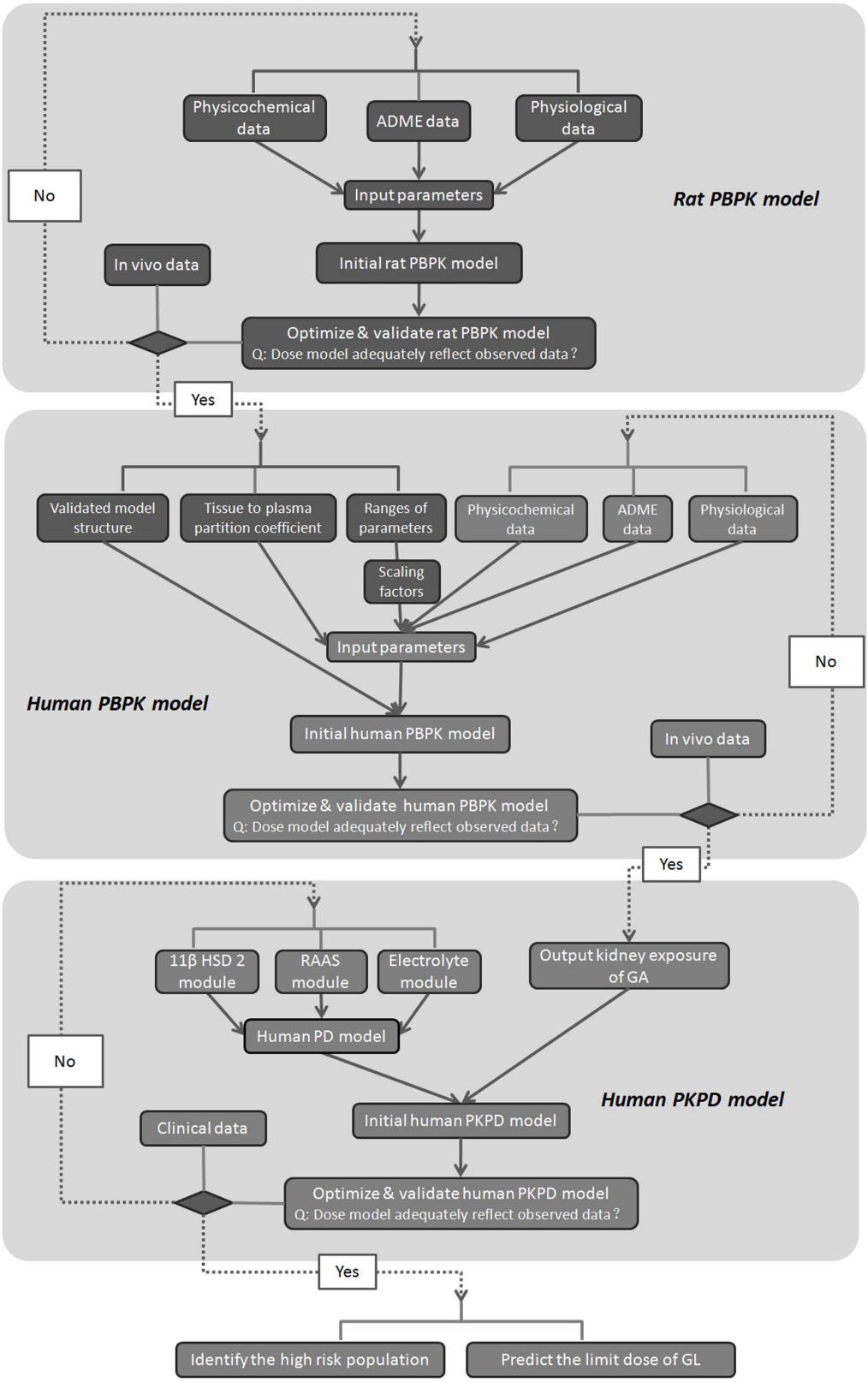

Figure 1. Work flow of PKPD modeling.

doi:10.1371/journal.pone.0114049.g001

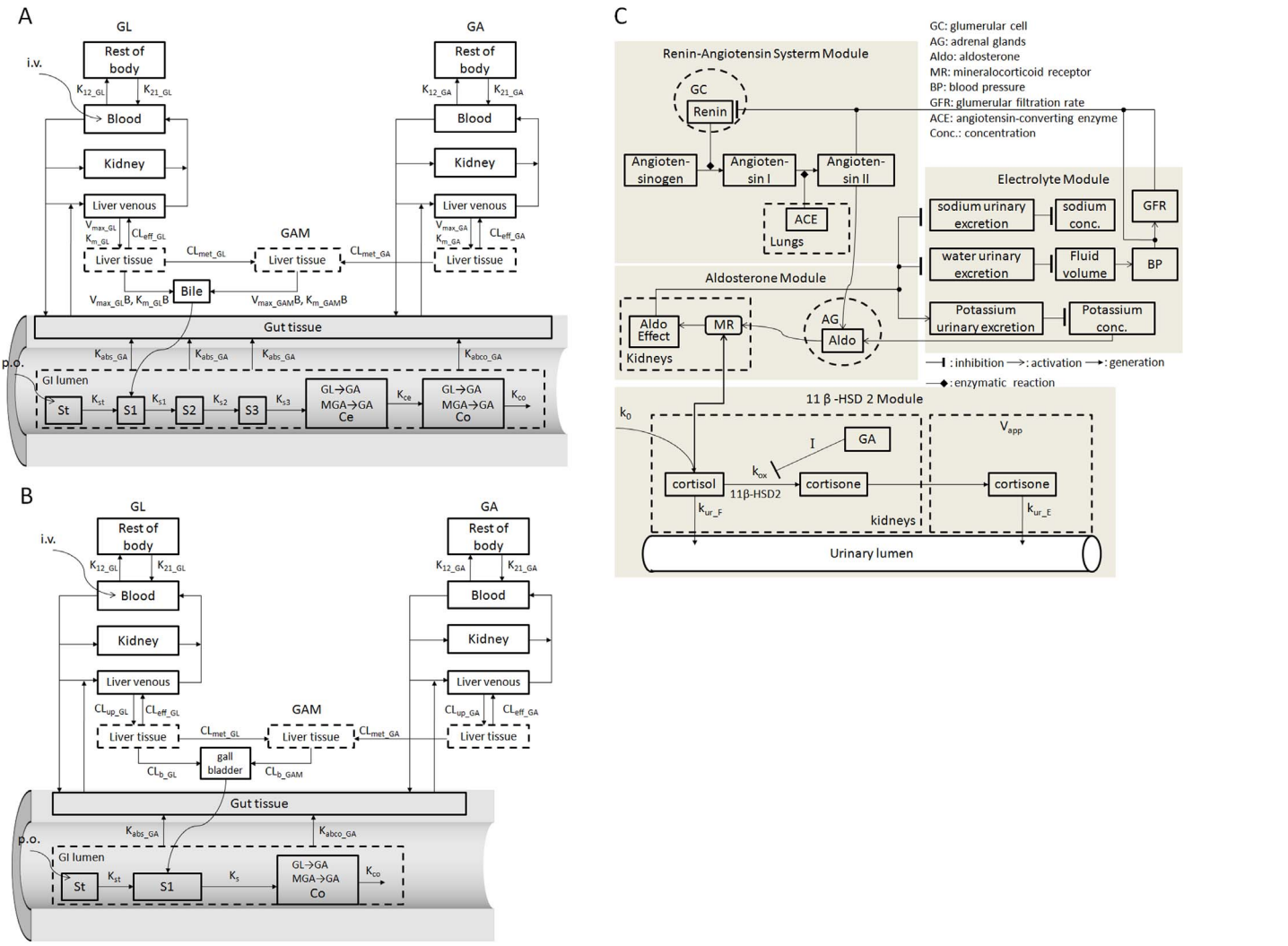

Figure 2. Model structure of the PKPD model. (A) Semi-PBPK model for the systemic kinetics of GL and GA in rat. (B) Semi-PBPK model for the systemic kinetics of GL and GA in human. (C)11β-HSD2 associated renin-angiotensin-aldosterone-electrolyte biological system PD model.

doi:10.1371/journal.pone.0114049.g002

scaling-induced extrapolation, we then developed the human PBPK model following similar steps as previously mentioned. After validation of the PBPK model, kidney exposure to GA in human was output and linked with the human PD model (consisting of three modules: 11β-HSD2 module, RAAS module and Electrolyte module). Finally, clinical indicators of pseudoaldosteronism could be predicted. The whole PBPK/PD model is developed step by step and validated during each step by observed data to prevent systematic errors.

Description of the GL model

The model consists of four tissue compartments and one blood compartment as shown in Figure 2A. The abbreviation of the parameters used in the PBPK models

Table 1. Abbreviations of parameters of the physiologically based pharmacokinetic model for GL, GA and GAM.

Abbreviation	Parameter
A_{abs}	Amount (μmol) of each compound absorbed from the gastrointestinal tract
A_x	Amount (μmol) of each compound in blood (x=v), kidney (x=k), hepatic venous (x=vl), liver (x=l), gut tissue (x=g), bile (x=b), or remaining tissue (x=r)
CL_{met}	Hepatic metabolic clearance (ml/h) of GL or GA
CL_x	Hepatic sinusoidal uptake clearance (x=up) and biliary excretion clearance (x=b) (l/h) of GL or GA in human
C_x	Concentration (μmol/ml) of each compound in blood (x=v), kidney (x=k), hepatic venous (x=vl), liver (x=l), gut tissue (x=g) or remaining tissue (x=r)
f_u	The unbound fraction of GL or GA in plasma
f_{ut}	The unbound fraction of GL, GA or GAM in tissue
K_{12_r}	Clearance (ml/h) of each compound distributed from blood to remaining tissue
K_{21_r}	Transit rate constant (h^{-1}) of each compound from remaining tissue to blood
K_{abs_x}	Absorption rate constant (h^{-1}) of each compound in small intestine (x=si) or colon (x=co)
KH_x	Hydrolysis rate constant (h^{-1}) of GL or GAM in cecum (x=ce) or colon (x=co)
K_m	Michaelis–Menten constant of each compound in hepatic sinusoidal uptake (μmol/ml)
K_x	Gastrointestinal transit rate constant (h^{-1}) in stomach (x=st), duodenum (x=sa), jejunum (x=sb), ileum (x=sc), cecum (x=ce) or colon (x=co) in rat model; or gastrointestinal transit rate constant (h^{-1}) in stomach (x=st), small intestine (x=s) or colon (x=co) in human model.
PS_{eff}	Hepatic sinusoidal efflux clearance of each compound (ml/h)
P_x	Tissue to plasma partition coefficient in kidney (x=k) or gut (x=g)
Q_x	Perfusion rate (ml/h) of kidney (x=k), hepatic artery (x=l) or portal vein (x=g)
V_{max}	Maximum hepatic sinusoidal uptake rate of each compound (μmol/h)
$V_{max}B$	Maximum biliary excretion rate of GL or GAM (μmol/h)

doi:10.1371/journal.pone.0114049.t001

are listed in Table 1. The kidney is the main target organ of GL-induced pseudoaldosteronism and has a high blood perfusion rate. The gut is isolated to describe the progress of absorption. Both of these tissues are assumed to be perfusion limited. As mentioned above, hepatic uptake and biliary excretion play important roles in GL elimination. GL has been shown to be actively transported into the liver by organic anion transport proteins (OATPs) [12] and subsequently excreted into the bile by multidrug resistance-associated protein 2 (MRP2) [13]. In order to model these processes, the liver was divided into a venous compartment and a tissue compartment and active transport of GL was described by a Michaelis–Menten-type equation. Besides biliary excretion, GL also undergoes passive diffusion from the liver into the plasma or is hydrolyzed to 3MGA by β-glucuronidase, both of which were assumed to be first order processes [14]. Then distribution in the remaining tissue was described by the parameters K_{12_r} and K_{21_r}. Since urinary excretion of GL and its metabolites accounts for only a small proportion (<2.5%) of the total drug [15, 16], renal clearance was ignored for GL and its metabolites.

Table 2. Physiological parameters in a 250 g rat and 70 kg human.

Tissue volume and blood flow[c]				
	rat		human	
Compartment	Volume (ml)	Blood flow rate (ml/h)	Volume (l)	Blood flow rate (l/h)
Liver	10.3	866.6[a]	1.8	90.9[a]
Guts	13.75[b]	762	1.15	71.5
Kidneys	1.875	553.8	0.3	69
Hepatic artery		104.6		19.4
Portal vein		762		71.5
Liver venous	1.2		0.18	
Vascular	18.75		5	

Gastrointestinal properties[d]			
Compartment	Transit time in rat (h)		Transit time in human (h)
Stomach	1.33		0.4 for liquid; 1.8 for solid
Small intestine	Part 1	0.33	3.3
	Part 2	0.67	
	Part 3	2.5	
Large intestine	cecum	7	15
	colon	7	

[a]Sum of hepatic artery plus portal vein flows.
[b]Sum of small intestine and large intestine.
[c]from literature [17].
[d]from literature [8, 9].

doi:10.1371/journal.pone.0114049.t002

Table 3. Biochemical parameters for the physiologically based model for GL, GA and GAM in rat.

Parameters	GL	GA	GAM	Source
K_{12_r}	20	143	—	fitted
K_{21_r}	0.46	1.6	—	fitted
f_u	0.006	0.008	—	[19]; [49]
f_{ut}	0.012	0.016	0.012	see text
Hematocrit	0.5	0.5	—	[19]
V_{max}	9.0	9.0	—	fitted
K_m	0.0014	0.0004	—	[22]; fitted
$V_{max}B$	4.7	—	4.7	fitted
K_mB	0.00037	—	0.00037	fitted
CL_{met}	737	2666	—	fitted; see text
PS_{eff}	26	411	—	[22]; see text
P_k	0.14	0.15	—	[18]
P_g	0.015	0.06	—	[18]; see text
$K_{abs,si}$	—	0.47	—	[24]; fitted
$K_{abs,co}$	—	0.58	—	[24]
KH_{ce}	0.29	—	0.03	[23]; see text
KH_{co}	0.11	—	0.03	[23]; see text

doi:10.1371/journal.pone.0114049.t003

Calibration of the GL model

Anatomical and physiological parameters taken from the literature [17] are listed in Table 2. Partition coefficients for each compartment [18] and the unbound fraction f_u of GL in plasma [19] are listed in Table 3. The unbound fraction of GL in tissue fu_t was estimated by equation (1) where fu_p is the unbound fraction in plasma, R is the average value of the tissue interstitial fluid-to-plasma ratio of albumin and lipoproteins (R=0.5 for lean tissues and R=0.15 for adipose tissue) [20, 21]:

$$fu_t = \frac{1}{1 + \frac{1-fu_p}{fu_p} \bullet R} \quad (R = 0.5) \tag{1}$$

The initial values of V_{max} and K_m for hepatic uptake were taken as the values determined in an isolated rat liver perfusion study [22]. As V_{max} and K_m can change simultaneously to keep the ratio constant, we here fixed K_m to the value obtained from the literature on the assumption that drug affinity would not change much in the perfused rat liver. Then V_{max}, K_{12_r} and K_{21_r} were optimized based on plasma concentration data and $V_{max}B$, K_mB and CL_{met} were optimized by curve fitting the accumulated biliary excretion data [15]. Since the oral bioavailability of GL is quite low (<4% in rat and cannot be detected in human) [5, 16, 23, 24], the absorption of GL after oral administration was ignored. The hydrolysis rate constant of GL (KH) in the large intestine was taken as the value determined by incubation of GL in gastrointestinal contents in vitro [23]. Other physiological parameters included in the gastrointestinal model were taken from the literature and are listed in Table 2 [17].

Description of the GA model

As in the GL model, four tissue compartments and one blood compartment were modeled to describe GA disposition in rat (shown in Figure 2A). The kidney and gut compartments were as described for the GL model. As nearly 100% of the radioactivity in a dose of tritium-labeled GA was found to be excreted into bile (mainly as metabolites) [25], it is clear that the liver plays an important role in the disposition of GA. GA can competitively inhibit the hepatic uptake of GL [26] indicating that the two compounds share the same sinusoidal transport system. When transported into the liver, GA is metabolized mainly by UDP-glucuronosyltransferase and sulfotransferases in what are supposedly first order processes. The resulting phase II metabolites (GAM) are then excreted with bile into the intestinal tract and hydrolyzed to GA which then undergoes enterohepatic recycling.

Calibration of the GA model

On the assumption that GA shares the same hepatic uptake transporter as GL, the V_{max} value which was considered to be related to the expression of the transporter

was taken to be the same as that in the GL model leaving K_m to be optimized. The metabolic clearance of GA by the human liver ($CL_{in\ vivo,\ human}$) was estimated based on its metabolism by human liver microsomes (HLM) in vitro [27] and further adjusted by the unbound fraction of drug in the incubation medium f_{u_inc} using equations 2 and 3 where logD is the measure of lipophilicity of the compound [28].

$$CL_{int,vivo,human} = \left(\frac{V_{max}}{K_m}\right)_{HLM} \bullet microsome\_protein/g\_liver \bullet liverweight/f_{u\_inc} \quad (2)$$

$$\log\left(\left(1-f_{u\_inc}\right)/f_{u\_inc}\right) = 0.53\log D - 1.42 \quad (3)$$

The metabolic clearance of GA by the rat liver ($CL_{int\ vivo,\ rat}$) was then estimated by scaling on the basis if liverweight as given in equation 4:

$$CL_{int,vivo,rat} = CL_{int,vivo,human} \bullet \frac{Liverweight_{rat}}{Liverweight_{human}} \quad (4)$$

The absorption rate constants of GA in each intestinal segment were obtained by the in situ loop method provided by Ploeger et al [8, 24]. The efflux clearance of GA from the liver to the venous blood (CL_{eff}) was assumed to be 15.6-fold greater than that of GL based on the fact that the passive permeability of GA in the gut lumen was estimated to be 15.6-fold greater than that of GL [24]. The data set of concentration-time profiles after i.v. administration of different doses of GA to rats with bile fistulas was used to optimize the parameters K_m, K_{12_r} and K_{21_r} [29]. Like GL, the biliary excretion of GAM is via Mrp2 [5] for which $V_{max}B$ and K_mB were assumed to be the same as those of GL and was validated using experimental data for: (1) The accumulated biliary excretion of 3MGA after i.v. administration of 3MGA at 5 mg/kg [5]; and (2) the accumulated biliary excretion of GAM after i.p. administration of GA at 25 mg/kg [25]. Then the colonic hydrolysis rate constant of GAM (KH_{GAM}) was optimized according to the plasma concentration-time profiles of GA after i.v. administration of GA at 5.7 mg/kg in rats without bile fistulas [30]. All other parameters were obtained from the literature and are listed in Table 3.

Equations for the PBPK models of rat and human are listed in detail in the Appendix S1.

Validation

The PBPK model in rat was further validated for the following scenarios: 10 mg/kg i.v., 25 mg/kg i.v. and 100 mg/kg i.v. GL [18, 19, 31]; 25 mg/kg i.p., 60 mg/kg i.v., and 5.7 mg/kg p.o. GA [18, 25, 30]; 10 mg/kg p.o. [30], 100 mg/kg p.o. and 200 mg/kg p.o. GL (experimental studies). The details are shown in the Results section.

Development of human PBPK model for GL and GA: from rat model to human model

The structure of the model of GL and its metabolites in human is similar to that in rat shown in Figure 2B. As the absorptive properties of the compounds in the different regions of the gastrointestinal tract are unclear, we divided the gastrointestinal tract into only three parts viz the stomach, small intestine and large intestine. The physiological parameters in human are listed in Table 2. Moreover, in the human model, GL and GAM are stored in the gallbladder from which they undergo biliary excretion into the intestinal lumen after the ingestion of fat at meal times [9]. The rate constants for hydrolysis of GL and GAM in the gut lumen were calculated based on the literature [32] and K_{12_r} and CL_{met} in the human model were scaled from those in the rat model based on the cardiac output and liver weight respectively. Tissue to plasma partition coefficients for kidney (P_k) and gut (P_g) in human were assumed to be the same as those in rat.

The initial values of CL_{up} and CL_b in the human model were extrapolated from the corresponding clearances in the rat model using the allometric equations 5 and 6 where BW_{rat} and BW_{human} are the body weights of rat (250 g) and human (70 kg) respectively:

$$CL_{up,human} = \left(\frac{V_{\max}}{K_m}\right)_{rat} \bullet \left(\frac{BW_{human}}{BW_{rat}}\right)^{\frac{3}{4}} \quad (5)$$

$$CL_{b,human} = \left(\frac{V_{\max}B}{K_mB}\right)_{rat} \bullet \left(\frac{BW_{human}}{BW_{rat}}\right)^{\frac{3}{4}} \quad (6)$$

The absorption rate constant of GL during enterohepatic recycling in human was obtained from the literature [19]. CL_{up} and CL_b of GL were then optimized according to plasma concentration-time data for a single 120 mg i.v. dose of GL. The simulated profiles following other i.v. doses of 40 and 80 mg [16] were compared with the observed data to further validate the model.

CL_{up} and the absorption rate constant (K_{abs}) of GA were optimized according to plasma concentration-time data for a single 130 mg p.o. dose [10]. The values were further validated for the following scenarios: Multiple p.o. administration of GA at 130 mg/day for 5 days [10]; a single p.o. administration of 225 mg GL; and a single p.o. administration of licorice equivalent to 225 mg GL [9]. For the licorice dose, the gut microbiota-mediated hydrolysis rate constant (KH) was assumed to be 4-fold greater since other components in licorice increase the extent of hydrolysis as shown in an in vitro study in rat [23].

Development of the pharmacodynamic model in human

As mentioned previously, GA reversibly inhibits 11β-HSD 2 in the kidney and gives rise to pseudoaldosteronism. The scheme of the PD model for the 11β-HSD 2 associated renin-angiotensin-aldosterone electrolyte system is shown in Figure 2C. The 11β-HSD 2 module was first developed from the Ploeger model

with some modification. The reversible inhibition of the conversion of cortisol into cortisone by GA can be described by the previously developed inhibitory Imax model [10],

$$I = \frac{I_{\max} \bullet C_{t\arg et,GA}}{IC50_{GA} + C_{t\arg et,GA}} \tag{7}$$

where C is the concentration of GA in the kidney and IC50 is the concentration producing 50% of the maximum inhibition. The initial value of IC50 was assumed to be equal to the corresponding value found in rat kidney microsomes i.e. 0.32 μM [33]. Kidney exposure to cortisol was described by equation 8:

$$\frac{dF_k}{dt} = (k_0 - F_k \bullet (k_{ox,0} \bullet (1 - I) + k_{ur\_F}))/V_k \tag{8}$$

where F_k is the kidney concentration of cortisol in human, k_0 is the rate of cortisol formation (assumed to be constant), V_k is the kidney volume and k_{ox} and k_{ur_F} are the 11β-HSD 2 metabolic clearance and urinary clearance of cortisol, respectively. For simplicity, we assumed that the elimination of cortisol takes place by these two pathways only. We also assumed that the change in cortisone concentration in plasma was only due to its formation by 11β-HSD 2-mediated oxidation of cortisol and urinary excretion. Accordingly, the change in plasma concentration of cortisone was described by equation 9:

$$\frac{dE}{dt} = (F_k \bullet k_{ox,0} \bullet (1 - I) - E \bullet k_{ur\_E})/V_{app} \tag{9}$$

where k_{ur_E} is the urinary clearance and V_{app} is the apparent distribution volume according to the plasma cortisone concentration. As the urinary cortisol:cortisone ratio is the generally accepted biomarker of 11β-HSD 2 inhibition, the urinary content of cortisol and cortisone were calculated as follows:

$$\frac{dF_u}{dt} = F_k \bullet k_{ur\_F}; \tag{10}$$

$$\frac{dE_u}{dt} = E \bullet k_{ur\_E} \tag{11}$$

and the 24 h urinary cortisol:cortisone ratio (R) was described as:

$$R = \frac{\int_{0-24} (F_k \bullet k_{ur\_F}) dt}{\int_{0-24} (E \bullet k_{ur\_E}) dt} \tag{12}$$

The parameters k_{ur_F} and k_{ur_E} were determined from the baseline 24 h urinary excretions of cortisol and cortisone [34] using the following equations:

$$k_{ur\_F}(L/h) = \frac{urinary\_excretion\_rate(nmol/day)/24}{F_{k0}(nmol/L)} \tag{13}$$

$$k_{ur\_E}(L/h) = \frac{urinary\_excretion\_rate(nmol/day)/24}{E_0(nmol/L)} \quad (14)$$

$$\text{where } F_{k0} = F_0 \bullet K_{tp\_cortisol} \quad (15)$$

F_0 and E_0 are the baseline plasma concentrations of cortisol and cortisone respectively, F_{k0} is the baseline kidney concentration of cortisol and $K_{tp\_cortisol}$ is the kidney:plasma concentration ratio of cortisol [35]. When GL is absent and equilibrium has been reached, equation 16 can be derived from equation 9:

$$F_{k0} \bullet k_{ox,0} = E_0 \bullet k_{ur\_E} \quad (16)$$

and equation 17 from equation 8:

$$k_0 = F_{k0} \bullet (k_{ox,0} + k_{ur\_F}) \quad (17)$$

The IC50 and V_{app} value were optimized based on the 24 h cortisol:cortisone ratio for 10 days after the first day of daily consumption of GA at 130 mg/day for five days.

Once 11β-HSD 2 is inhibited, the increased concentration of cortisol activates the MR and further induces sodium and water retention, hypokalemia, and hypertension. Ikeda et.al [36] developed a comprehensive network for overall regulation of body fluids which we used with some modification in the present study as the electrolyte module to predict the serum potassium and sodium levels. Moreover, several studies have reported that a significant suppression of the renin-angiotensin-aldosterone axis occurs after over-consumption of licorice and GA taken to be a compensatory response to the excessive activation of the MR by cortisol [34, 37]. Guillaud and Hannaert [38] developed a computational model of the renin-angiotensin system which can output the plasma renin, angiotensin I and angiotensin II levels but not aldosterone level, and successfully predicted the effect of renin inhibitor aliskiren. We then developed the mathematical relationship between aldosterone and angiotensin II given in equation 18 and further linked it with the Ikeda model shown in Figure 2C. Since angiotensin II and potassium are primary secretagogues modifying aldosterone release [39], we assumed that generation and secretion of aldosterone are mainly regulated by the two factors shown in equation 18 (i.e. the generation of Aldo stimulated by Angiotensin II and potassium in Figure 2C). Here K_{gen_aldo} and K_{deg_aldo} are the zero-order release rate constant and first-order elimination rate constant of aldosterone, S_{max} is the maximum stimulation, SC50 is the concentration producing 50% of maximum stimulation and r is the Hill coefficient. These parameters were obtained by curve fitting the experimental data [40, 41]. The RAAS is further regulated by the arterial pressure, venous pressure and glomerular filtration rate (GFR) which can be outputs of the Ikeda model [38].

$$\frac{d([Aldo])}{dt} = K_{gen\_aldo} \bullet (1 + \frac{S_{\max} \bullet [K^+]^r \bullet [AngII]}{(SC50_{K^+}{}^r + [K^+]^r) \bullet (SC50_{AngII} + [AngII])}) - K_{\deg\_aldo} \bullet [Aldo] \quad (18)$$

The body fluids model developed by Ikeda consists of 7 blocks, 5 of which were the main focus of the present study and are described briefly as follows: Block 1, the cardiovascular system, calibrates the relationship between blood volume and systemic arterial and venous pressure; Block 3, the extracellular space, calibrates the changes in water in the vascular and extracellular space; Block 4, the intracellular space and electrolytes, calibrates the potassium and sodium concentrations in extracellular fluids; Block 6, the kidney, calibrates the urinary excretion of water, sodium and potassium; and Block 7, the controller of renal function, calibrates GFR. Block 2 and 5 correspond to the predictions of the respiratory system and urinary anion excretion respectively which are not the main outputs in our model. The Ikeda model was described mathematically as a set of nonlinear differential and algebraic equations of more than 200 variables. Behavior of the model for various kinds of inputs simulated with a digital computer was in good agreement with a number of experimental results pertaining to body fluids and electrolytes [36]. The scheme of the renin-angiotensin-aldosterone-electrolyte network model modified on the basis of the original literature [36, 38] is shown in Figure 2C with equations given in detail in Appendix S2. The effect of cortisol on the MR was added to the aldosterone effect in the electrolyte module as indicated in equation 19 (i.e. the stimulation of MR by Aldo and cortisol in Figure 2C):

$$ALD_0 = \frac{[Aldo] - [Aldo]_0}{[Aldo]_0} + \frac{[F_k] - [F_k]_0}{[F_k]_0} \quad (19)$$

where ALD_0 is a normalized value presenting the effect of MR defined by Ikeda et al. and $[Aldo]_0$ and $[F_k]_0$ are the baseline concentrations of aldosterone in plasma and cortisol in kidney respectively. ALD_0 then affects the urinary excretion of potassium and sodium (YKU and YNU) in Block 6 of the Ikeda model. Finally the electrolyte module outputs the serum potassium and sodium levels.

Simulation software

All simulations were performed using MATLAB (the MathWorks Inc., Natick, MA, USA). The PKPD model was constructed as a set of ordinary differential equation (ODEs), the integration of which was performed using the fourth order Runge-Kutta method. The accuracy of the prediction was graphically evaluated by superimposing the concentration–time profile observed *in vivo* to the simulated ones.

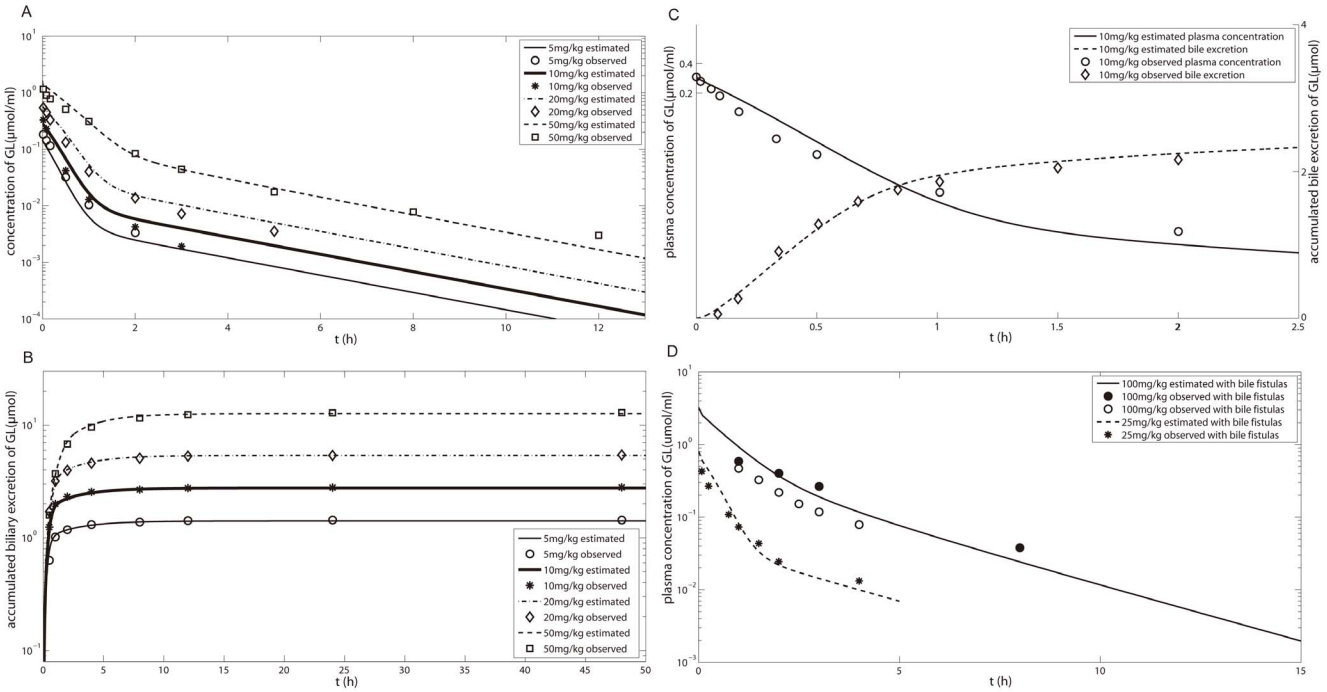

Figure 3. GL plasma concentration and accumulated biliary excretion after i.v. GL in rats with bile fistulas. Plasma concentration-time profiles of GL at (A) 5–50 mg/kg [15], (C) 10 mg/kg [13], (D) 25 and 100 mg/kg [18, 19, 31]; accumulated biliary excretion of GL at (B) 5–50 mg/kg [15] and (C) 10 mg/kg [13]. Experimental data (fitset and testset) are shown as symbols; the lines represent the prediction of the GL model.

doi:10.1371/journal.pone.0114049.g003

Results

PBPK modeling of GL and its metabolites in rat

In this study, a PBPK model was developed to predict the PK profiles of GL and GA after i.v. and p.o. administrations. Drug specific parameters used to develop the semi-PBPK model are listed in Table 3. Optimization of the parameters K_{12}, K_{21}, V_{max}, $V_{max}B$, K_mB and CL_{met} in the GL model according to plasma concentration-time profiles and accumulated biliary excretion are shown in Figure 3A–B. It can be seen that the predicted lines give a good fit to the observed data. The optimized value of V_{max} (8.96 μmol/h) is quite close to that (10.1 μmol/h) calculated from isolated liver perfusion experiments, indicating that fixing K_m to the experimental value was a reasonable strategy. We further simulated different scenarios of i.v. administration of GL [18, 19, 31] and validated the model by comparing the simulations with data reported in the literature (Figure 3C–D). The results show that the simulated and reported profiles are comparable.

Curve fitting of K_m, k_{12} and k_{21} in the GA model to concentration-time profiles for i.v. administration of 2–20 mg/kg GA to rats with bile fistulas is shown in Figure 4A. Curve fitting of the 3MGA plasma concentration-time profile and subsequent simulation of its biliary excretion after i.v. administration of 3MGA at 5 mg/kg [5] and of GAM biliary excretion after i.p. administration of GA at

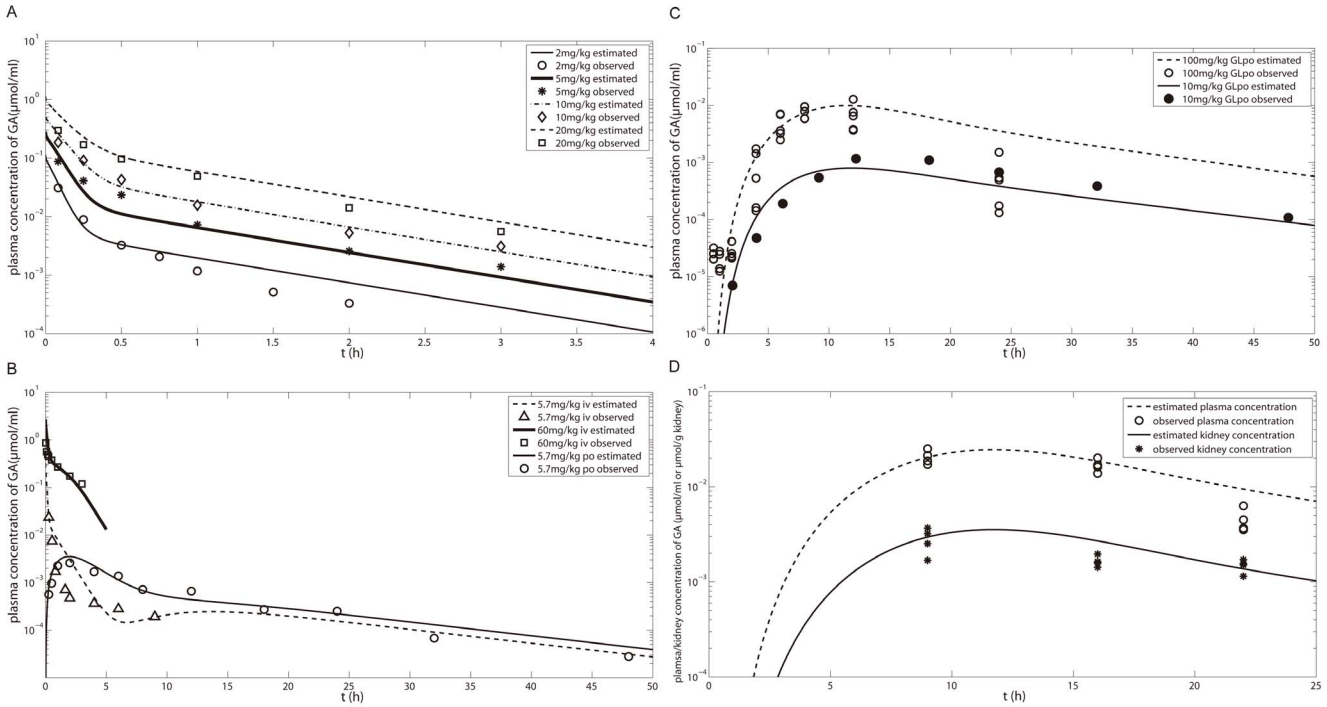

Figure 4. GA plasma and kidney concentration after i.v. GA and p.o. GA and GL in rats. (A) Plasma concentration-time profiles of GA after i.v. 2–20 mg/kg GA in rats with bile fistulas [29]; (B) i.v. 60 mg/kg GA in rats with bile fistulas [18], i.v. 5.7 mg/kg GA in rats without bile fistulas and p.o. 5.7 mg/kg GA in rats [30]; (C) p.o. 10 [30] and 100 (experimental studies) mg/kg GL; (D) plasma and kidney exposure of GA after p.o. 200 mg/kg GL (experimental studies). Experimental data (fitset and testset) are shown as symbols; the lines represent the forecast of the GA model.

doi:10.1371/journal.pone.0114049.g004

25 mg/kg [25] are shown in Figure 5. After optimization of KH_{GAM} by curve fitting of plasma concentration-time data for GA administration (i.v. 5.7 mg/kg [30]), the GA model was further validated for the following scenarios: 60 mg/kg i.v. [18] and 5.7 mg/kg p.o. GA; 10 mg/kg p.o. [30] and 100 mg/kg p.o. GL (experimental studies) shown in Figure 4B–C. Finally we simulated the kidney and plasma exposure to GA after p.o. administration of 200 mg/kg GL (experimental study) and compared the results with the observed data as shown in Figure 4D. The results show that the model predicts well the kidney exposure to GA which guarantees a reliable input into the PD model.

PBPK modeling of GL and its metabolites in human

The estimated PK profiles following three i.v. doses of GL were comparable with literature data as shown in Figure 6A. In the GA model, the CL_{up} value and rate constants for absorption in the small intestine and colon were optimized based on the plasma concentration-time profile for p.o. administration of GA (Figure 6B). Simulation of the PK profiles of GA for the three scenarios of administration mentioned in the Methods (Figure 6B–C) illustrates that the model gives good predictions for the different scenarios. The drug specific parameters of the human PBPK model are listed in Table 4.

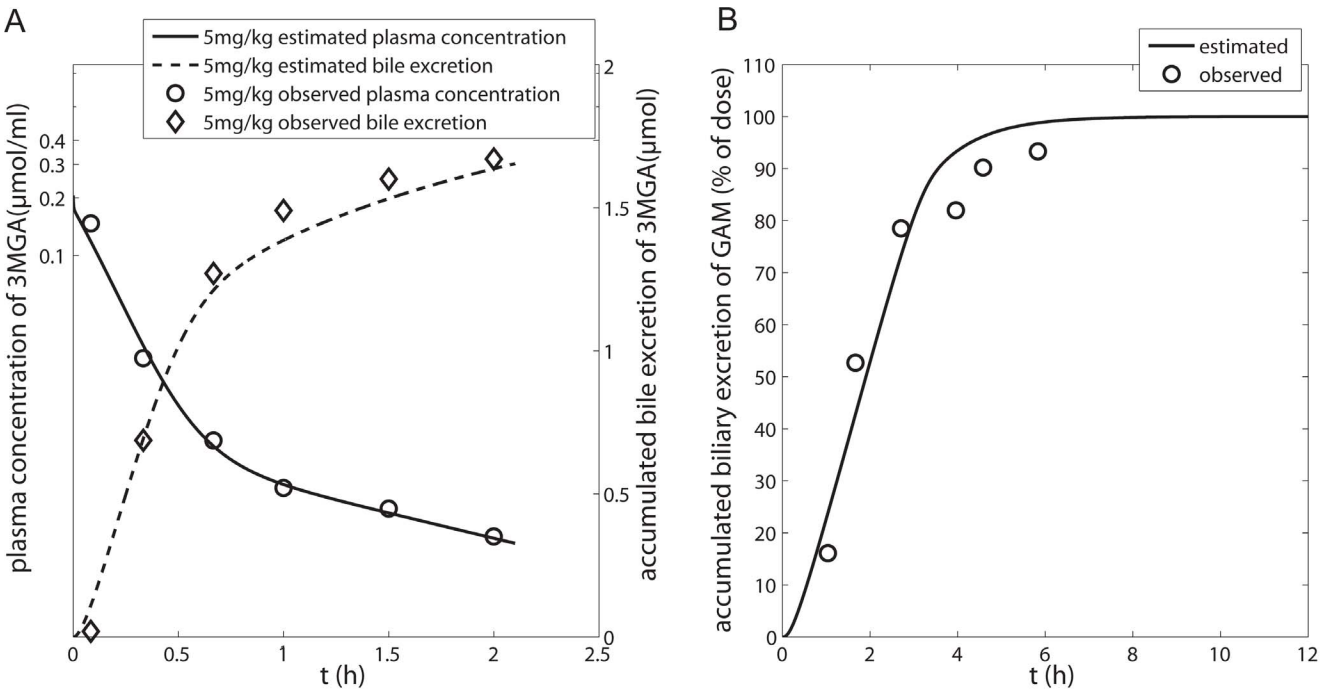

Figure 5. Plamsa concentration and accumulated biliary excretion of GAM. Left, plasma concentration and accumulated biliary excretion of 3MGA after i.v. 5 mg/kg 3MGA in rats [5]; Right, accumulated biliary excretion of GAM after i.p. 25 mg/kg GA in rats [25]. Experimental data are shown as symbols; the lines represent the predictions of the GA model.

doi:10.1371/journal.pone.0114049.g005

PK/PD modeling for prediction of the adverse effects of GL in human

The human PK/PD model was constructed in two stages: the first to predict the urinary cortisol:cortisone ratio (11β-HSD 2 module), the second to estimate the levels of serum potassium and sodium, plasma aldosterone etc. in the RAAS and electrolyte modules.

Figure 7A shows the results of optimization of the IC50 and V_{app} values based on the observed 24 h urinary cortisol:cortisone ratio after p.o. administration of 130 mg/day GA for five days. The optimized parameters are listed in Table 5. Validation and simulation of the urinary cortisol:cortisone ratio were further carried out for the following two scenarios: (1) Multiple p.o. administrations of 250 mg GA twice a day for 7 days (Figure 7D); and (2) multiple p.o. administrations of 170 mg GA three times a day for 2 days (Table 6). In the first scenario, we also simulated the 24 h urinary excretion of cortisol and cortisone and compared the results with the observed data (Figure 7B–C). It was found that the predicted and observed data were comparable indicating the resulting model was robust. Curve fitting the aldosterone model with the experimental data is shown in Figure 8A–B and the optimized parameters are listed in Table 5.

We then predicted the changes in the RAAS and serum electrolyte levels after p.o. administration of GA and licorice. The results shown in Tables 7 and 8 suggest that the RAAS was significantly inhibited presumably as a compensatory

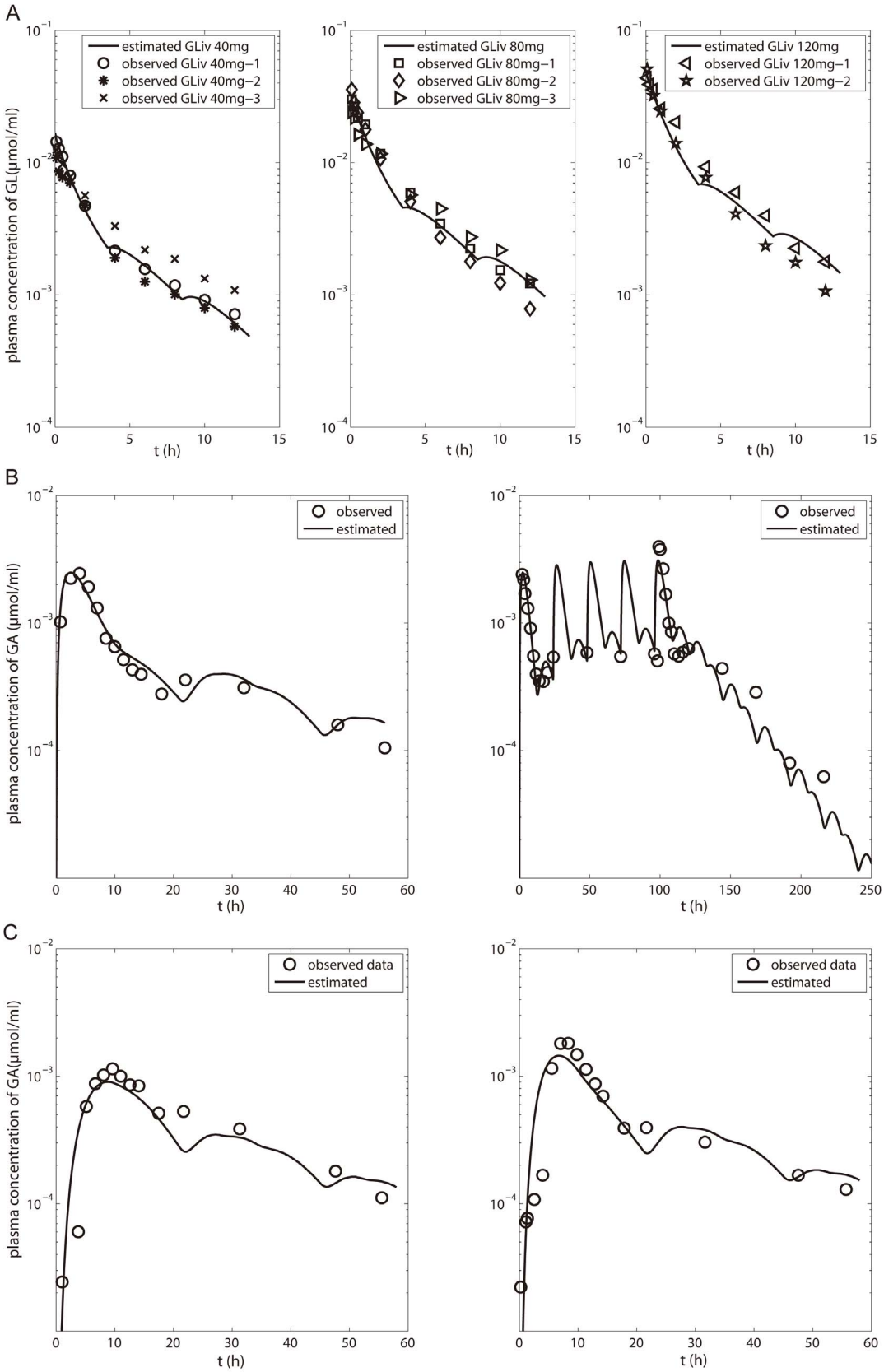
A
estimated GLiv 40mg
observed GLiv 40mg−1
observed GLiv 40mg−2
observed GLiv 40mg−3
estimated GLiv 80mg
observed GLiv 80mg−1
observed GLiv 80mg−2
observed GLiv 80mg−3
estimated GLiv 120mg
observed GLiv 120mg−1
observed GLiv 120mg−2
plasma concentration of GL(μmol/ml)
t (h)
B
observed
estimated
plasma concentration of GA (μmol/ml)
t (h)
C
observed data
estimated
plasma concentration of GA(μmol/ml)
t (h)

Figure 6. Plasma concentrations of GL and GA in human. (A) GL plasma concentration after i.v. 40–120 mg GL in human [16]; (B) GA plasma concentration after p.o. administration of 130 mg/kg GA at (B, left) single dose and (B, right) multiple dose [10]; GA plasma concentration after p.o. (C, left) 225 mg GL and (C, right) 150 g licorice containing 225 mg GL [9]. Experimental data (fitset and testset) are shown as symbols; the lines represent the predictions of the human PBPK model.

doi:10.1371/journal.pone.0114049.g006

mechanism for over-activation of the MR as supported by experimental data from several studies. The predicted results after one and four weeks in the second scenario indicate that plasma levels of the indicators of GL-induced pseudoaldosteronism significantly declined in the first week consistent with the description in the literature. The predicted and observed values were all comparable showing that the indicators of pseudoaldosteronism are well predicted by the present PKPD model.

Identification of the important factors relating to GL-induced pseudoaldosteronism

We further investigated the effects of changes in sinusoidal transport function, colonic transit time and activity of 11β-HSD 2, all of which have been reported to display high inter-individual variability, on the PK of GA and serum potassium level (chosen as the indicator of pseudoaldosteronism) after p.o. administration of 200 mg/kg GL in human.

As mentioned above, hepatic clearance is the major elimination pathway of GA and, according to the parameters in the PBPK model of GA, hepatic sinusoidal uptake clearance (20000 l/h) is almost 1000 times greater than sinusoidal efflux clearance (28.18 l/h) meaning sinusoidal uptake rather than intrinsic hepatic metabolism is the determinant of hepatic disposition. Moreover, expression of the hepatic sinusoidal OATP transporters shows a large inter-individual variability

Table 4. Biochemical parameters of the physiologically based model for GL, GA and GAM in human.

Parameter	GL	GA	GAM	Source
K_{12_r}	1241	9016	—	see text
K_{21_r}	0.13	0.46	—	see text
f_u	0.004	0.0008	—	[19]; [49]
f_{ut}	0.008	0.0016	0.008	see text
Hematocrit	0.42	0.42	—	[19]
CL_{up}	431	20000	—	see text
CL_b	454.0	—	454	see text
CL_{met}	50516	371546	—	see text
PS_{eff}	1809	28179	—	see text
P_k	0.14	0.15	—	see text
P_g	0.015	0.06	—	see text
$K_{abs,si}$	0.13	0.084	—	[19]; fitted
$K_{abs,co}$	—	0.40	—	fitted
KH_{co}	0.19	—	0.1	[32]

doi:10.1371/journal.pone.0114049.t004

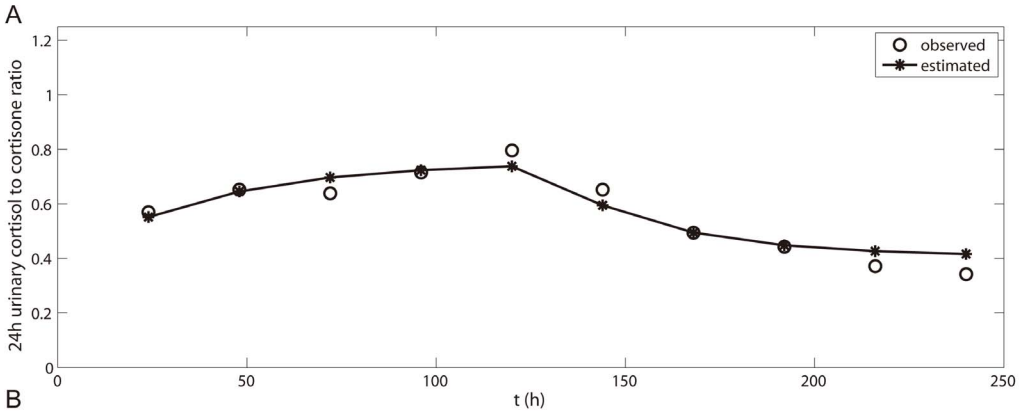
A
24h urinary cortisol to cortisone ratio
t (h)
observed
estimated

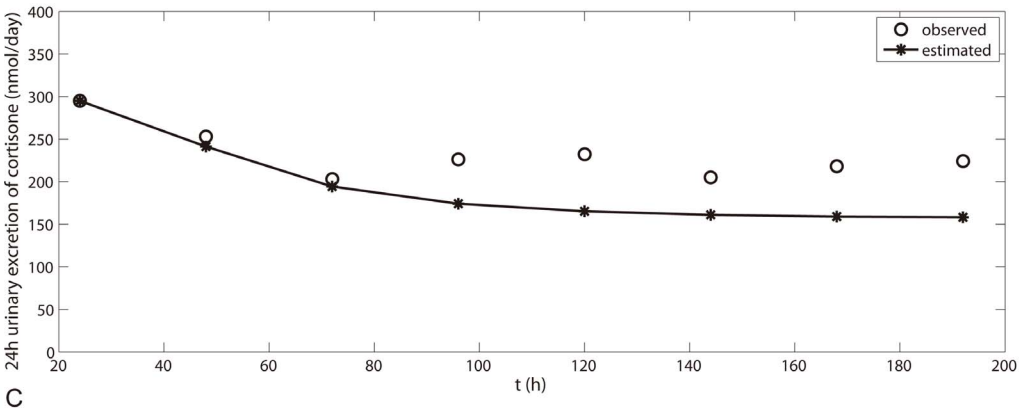
B
24h urinary excretion of cortisone (nmol/day)
t (h)
observed
estimated

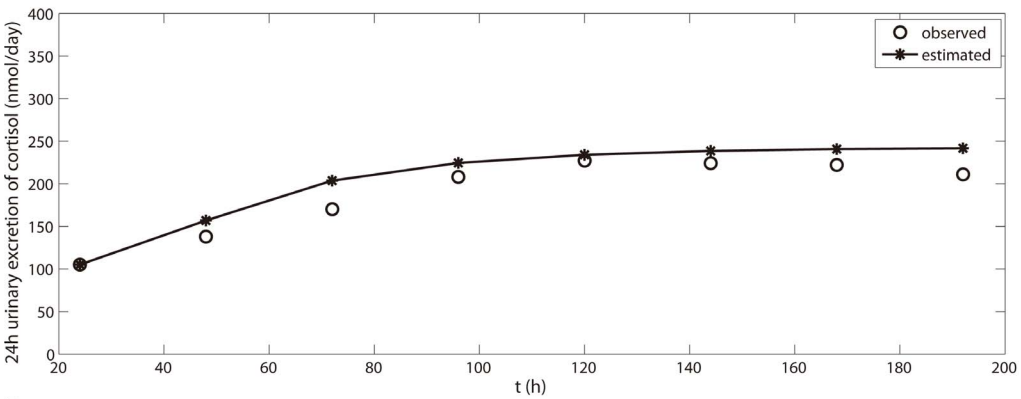
C
24h urinary excretion of cortisol (nmol/day)
t (h)
observed
estimated

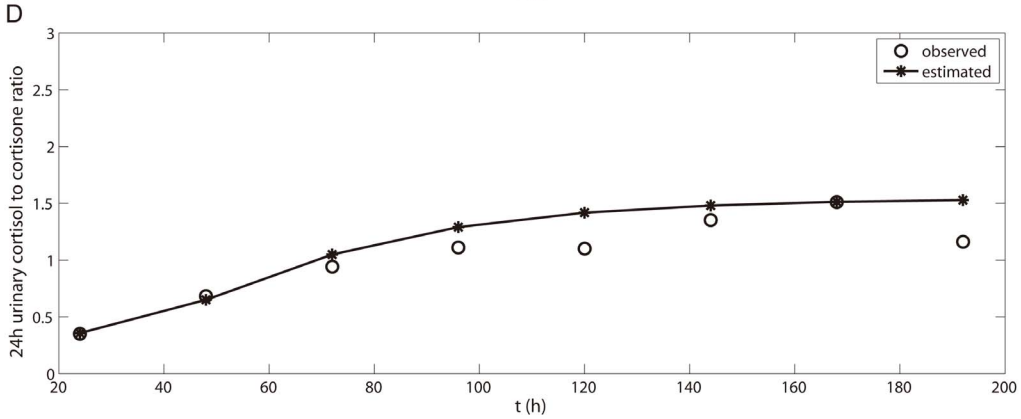
D
24h urinary cortisol to cortisone ratio
t (h)
observed
estimated

Figure 7. Time courses of urinary excretion of cortisol, cortisone and their ratio in different scenarios: (A) p.o. GA 130 mg/day for 5 days and withdrawn for another 5 days [10]; (B–D) p.o. GA 500 mg/day, 2 times/day for 7 days [34].

doi:10.1371/journal.pone.0114049.g007

suggesting that hepatic sinusoidal uptake function may contribute to the inter-individual variability in GL-induced adverse effects. CL_{up} is proportional to the V_{max} of the uptake process which is further supposedly proportional to the expression of the sinusoidal transporter. OATP1B1 and OATP1B3 are the major transporters mediating GL and GA sinusoidal uptake in human and regulation of their expression, according to previous reports, is coordinated within an individual [42]. Thus, in the present study, the change in expression of OATP1B1 was taken as a measure of the change in CL_{up}. Details are as follows. According to a previous report [43], there is a 4.9-fold inter-individual variability in OATP1B1 mRNA expression level in the liver. Thus the median was set to the normal value N and two other values of CL_{up} (N/2.21 and 2.21*N) were chosen. The results (Figure 9A–B) show that a decrease in CL_{up} can significantly increase exposure to GA and subsequently decrease the serum potassium level, indicating that a decrease in sinusoidal transport function increases sensitivity to GL-induced adverse effects.

Since the adverse effect of GL is especially severe in elderly patients [44, 45] and since, according to previous reports, age is an important factor impacting colonic transit time and the activity of 11β-HSD 2 [46, 47], the effects of colonic transit time and activity of 11β-HSD 2 on the serum potassium level were further investigated. According to the reported values for colonic transit time and cortisol:cortisone ratio in the elderly, we set K_{co} and $k_{ox,0}$ to 0.0217 h^{-1} and 0.02 l/h respectively (the normal value of $k_{ox,0}$ is about 1.8 times greater), predicted the plasma exposure to GA and potassium levels for one week and further compared them with those of using normal values of K_{co} and $k_{ox,0}$. The results shown in Figure 9C–E suggest that a prolonged colonic transit time and a decrease in 11β-HSD 2 activity make subjects more susceptible to experiencing adverse effects and may explain why GL-induced pseudoaldosteronism mainly occurs in the elderly.

According to the literature mentioned above [43, 46, 47], the distribution of CL_{up} in the general population and K_{co} and $k_{ox,0}$ in the elderly can be estimated and are listed in Table 9. Using the Monte Carlo method, we further simulated the dose limit for 1000 virtual elderly subjects according to the known distribution of the above three parameters in the elderly. Based on the normal range of serum potassium of 3.5–5.0 mmol/l, the median value (4.18 mmol/l) was chosen as the typical normal value of serum potassium. A series of doses were simulated for each subject and the individual dose limit leading to hypokalemia was determined as the dose giving a serum potassium level of 3.5 mmol/l on the 28^{th} day. The results are shown in Figure 10A. The distribution was well described by a logarithmic normal distribution and the distribution parameters μ and σ were found to be 5.6348 and 0.5449 respectively. Moreover, in the left part of the

Table 5. Optimized parameters in the PD model.

Parameter	Optimized value
K_{gen_aldo} (ng/dl/h)	62.8
S_{max}	92.63
$SC50_{K^+}$ (mmol/l)	4.577
$SC50_{AngII}$ (pg/ml)	94.129
K_{deg_aldo} (h^{-1})	18.67
V_{app} (l)	5.2
$IC50_{GA}$ (μmol/ml)	0.000234
Γ	9.97

doi:10.1371/journal.pone.0114049.t005

cumulative probability curve shown in Figure 10B, there is a critical value point of around 100 mg representing the highest rate of change in the cumulative probability. We further calculated it as the maximum value in the second derivative of the cumulative probability distribution function and obtained a value of 101 mg (Figure 10C). This indicates that the risk of adverse effects increases abruptly above 101 mg making this the critical dose limit of GL causing hypokalemia in the elderly with a probability of 3.07%. We further estimated the probability of hypokalemia in the elderly for the upper dose limit recommended by SCF (100 mg/day) as 3% and DNIB (200 mg/day) as 27%. The results show that, although the dose is only doubled, the probability is unexpectedly 9 times higher. It is suggested that the risk of the adverse effect at the DNIB recommended dose (200 mg/kg) is substantially greater probably due to high popularity of licorice containing foods in the Netherlands.

Discussion

Consumption of GL in large amounts or for a long period of time leads to the adverse effects of pseudoaldosteronism which can be quite severe if ignored. In the present study, a semi-PBPKPD model was developed to predict the adverse effects of GL and facilitate its safe use both clinically and as a food additive.

Pseudoaldosteronism is caused by inhibition of 11β-HSD 2 by GA, the major metabolite of GL. Since the kidney is the target tissue for the adverse effects of GL, kidney exposure to GA is likely to be more important than systemic exposure and could be directly linked with the PD model. We made this prediction and validated it in the rat model and assumed that the plasma to kidney distribution

Table 6. Estimated urinary cortisol:cortisone ratio for p.o. administration of GA at 510 mg/day administered 3 times/day for 2 days compared with the observed value.

Dosage regimen	Time (day)	Observed value	Estimated value
GA p.o. 510 mg/day 3 times/day for 2 days	2	2.36 (0.69)[a]	2.0

[a]The observed value [50] is expressed as mean (SD). The baseline value before administration is 0.65 (0.06).

doi:10.1371/journal.pone.0114049.t006

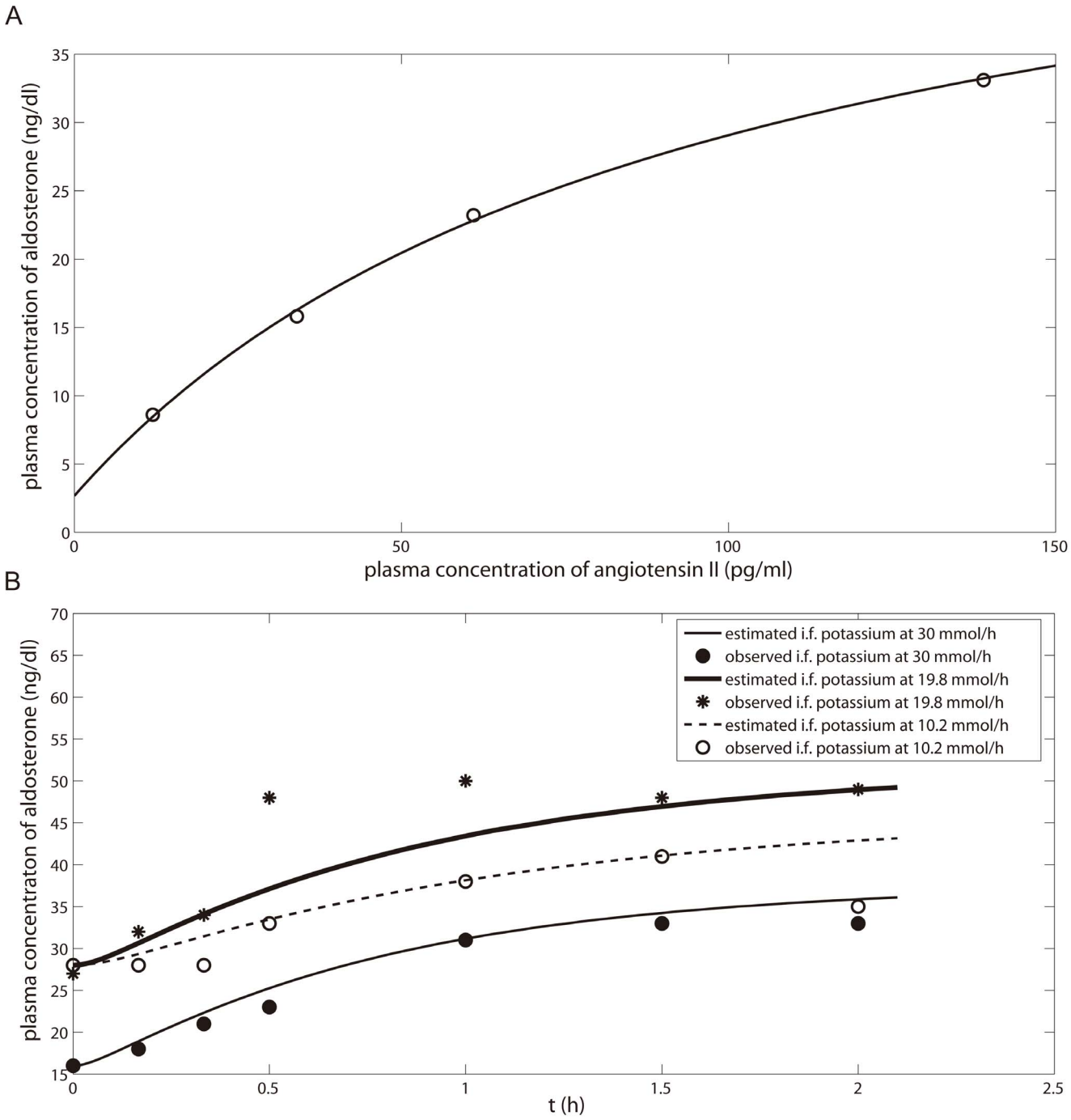

Figure 8. The effects of different levels of (A) angiotensin II [40] and (B) potassium [41] on aldosterone concentration. Experimental data (fitset) are shown as symbols; the lines represent the predictions of the human PBPK model. i.f. in B stands for intravenous infusion.

doi:10.1371/journal.pone.0114049.g008

in rat and human was the same. As a consequence, a semi-PBPK model was first developed in rat mainly to validate the model structure, clarify the mechanisms of action and provide reasonable parameters for the human model.

Table 7. Estimated biomarkers of pseudoaldosteronism for p.o. administration of GA at 500 mg/day 2 times/day for one week compared with the observed value.

	Base line	Observed value[a]	Predicted value
Aldosterone (ng/dl)	13.1 (2.7)	6.0 (3.5)	5.8
Sodium (mmol/l)	141 (0.5)	144 (0.6)	142
Potassium (mmol/l)	3.7 (0.09)	3.3 (0.04)	3.3

[a]The observed value [34] is expressed as mean (SE).

doi:10.1371/journal.pone.0114049.t007

The present liver model was developed mainly on the basis of Ishida's isolated perfused liver model in which the parameters of GL hepatic disposition were calculated from experimental data and used as initial values in optimization. The structure of the PBPK model can be simplified or complicated according to the objective based on a reasonable mechanism. According to our objective of identifying a high risk population in which sinusoidal transport may be an important factor causing variability in adverse effects, the present model connected sinusoidal uptake, intrinsic hepatic metabolism and biliary excretion in a tandem pattern allowing analysis of the impact of sinusoidal transport on exposure to GL and GA. In contrast, in Ploeger's PBPK model, partial sinusoidal uptake and biliary excretion were combined into one process, making it difficult to further analyze the rate sensitive process in drug elimination.

Simple exposure-response PD models cannot explain the complicated mechanisms involved in such things as signal transduction and feedback loops making it difficult to predict clinical indicators far from the site of action. A mechanistic model can, however, include factors and processes involved in well-clarified mechanisms of action making it possible to simulate clinical reality, to predict more than one indicator at the same time and to establish the quantitative relationship between target-related and end point-related indicators. Thus, in order to achieve this objective, we developed a mechanism-based PD model. The PD model was further divided into three parts: the 11β-HSD 2 module (target

Table 8. Estimated biomarkers of pseudoaldosteronism for p.o. administration of GL at 0.7 g/day (9 subjects) or 1.4 g/day (5 subjects) for one to four weeks compared with observed values.

	Base line		Time after dose	Observed value[a]		Predicted value		
						0.7 g/day	1.4 g/day	mean
Aldosterone (ng/dl)	21.5		1 week	7.1 (1.9)		11.0	7.5	9.8
			4 weeks	8.6 (4.2)		8.9	5.4	7.7
Angiotensin II (pg/ml)	54.4		1 week	42.1 (14.5)		42.6	32.4	40.0
			4 weeks	40.8 (22.0)		46.6	37.8	43.4
Potassium (mmol/l)	**0.7 g/day**	4.1	4 weeks	**0.7 g/day**	**1.4 g/day**	3.7	3.3	
	1.4 g/day	4.0		3.7(0.4)	3.4(0.2)			

[a]The observed value [37] is expressed as mean (SD).

doi:10.1371/journal.pone.0114049.t008

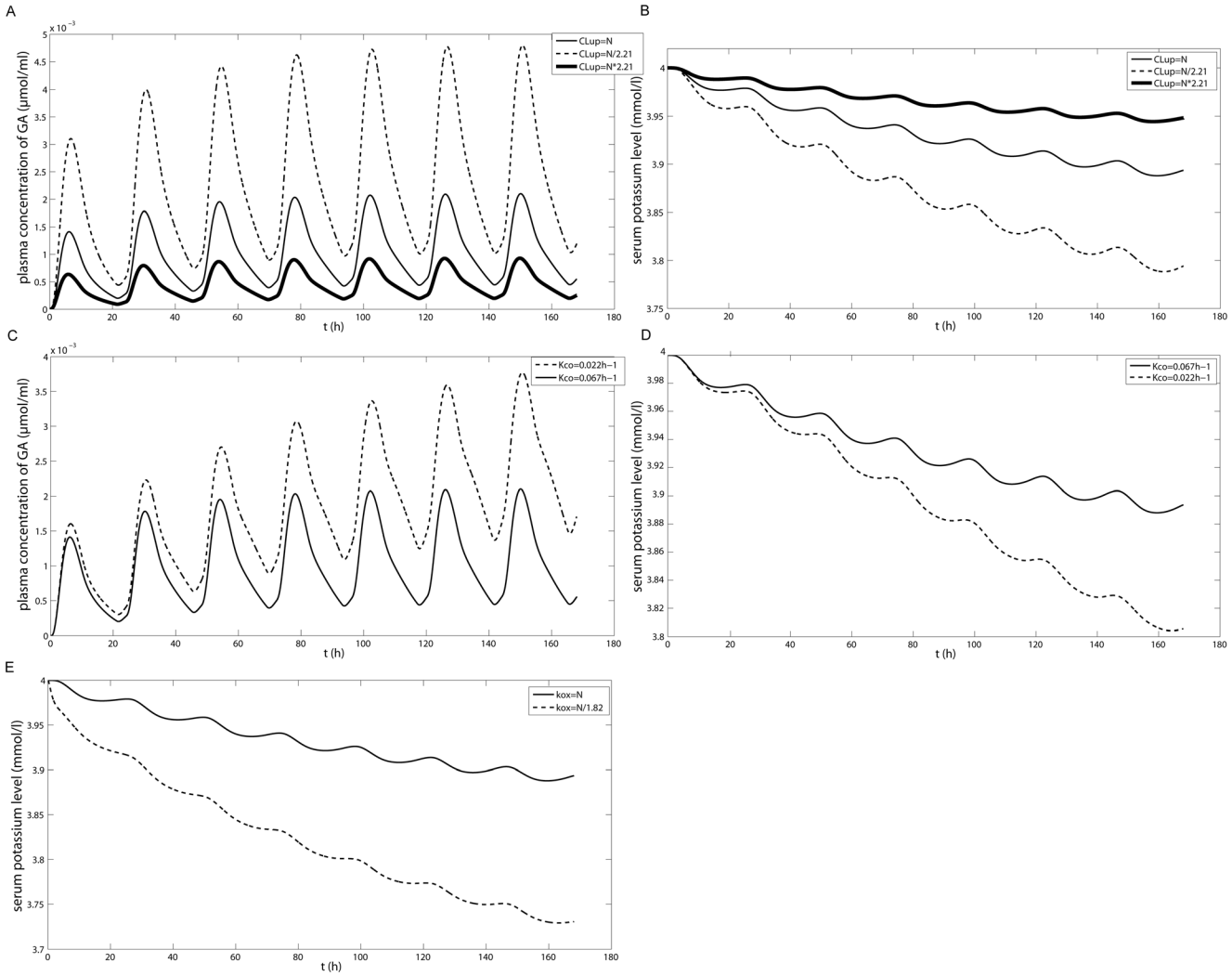

Figure 9. The simulated effect of three sensitivity factors on GA pharmacokinetics and potassium level. Sensitivity factors: (A, B) sinusoidal transport function, (C, D) colonic transit time and (E) activity of 11β-HSD 2. The causal effect: (A, C) GA plasma concentration and (B, D, E) serum potassium level. GL was administered p.o. at 200 mg/day for one week. N stands for the normal value of the corresponding parameter.

doi:10.1371/journal.pone.0114049.g009

Table 9. Distribution of CL_{up}, K_{co}, and $k_{ox,0}$ related physiological factors in simulation of the individual dose limit for 1000 subjects by the Monte Carlo method.

Physiological factor	Parameter	Number of samples	Estimation of the distribution	Sources
Expression of OATP1B1	CL_{up}	31	Log normal distribution	[43]
Colonic transit time	K_{co}	16	Bootstrapping	[46]
Plasma cortisol:cortisone ratio	$k_{ox,0}$	21	Truncated normal distribution[a]	[47]

[a]The boundary is according to the extreme value for 21 samples.

doi:10.1371/journal.pone.0114049.t009

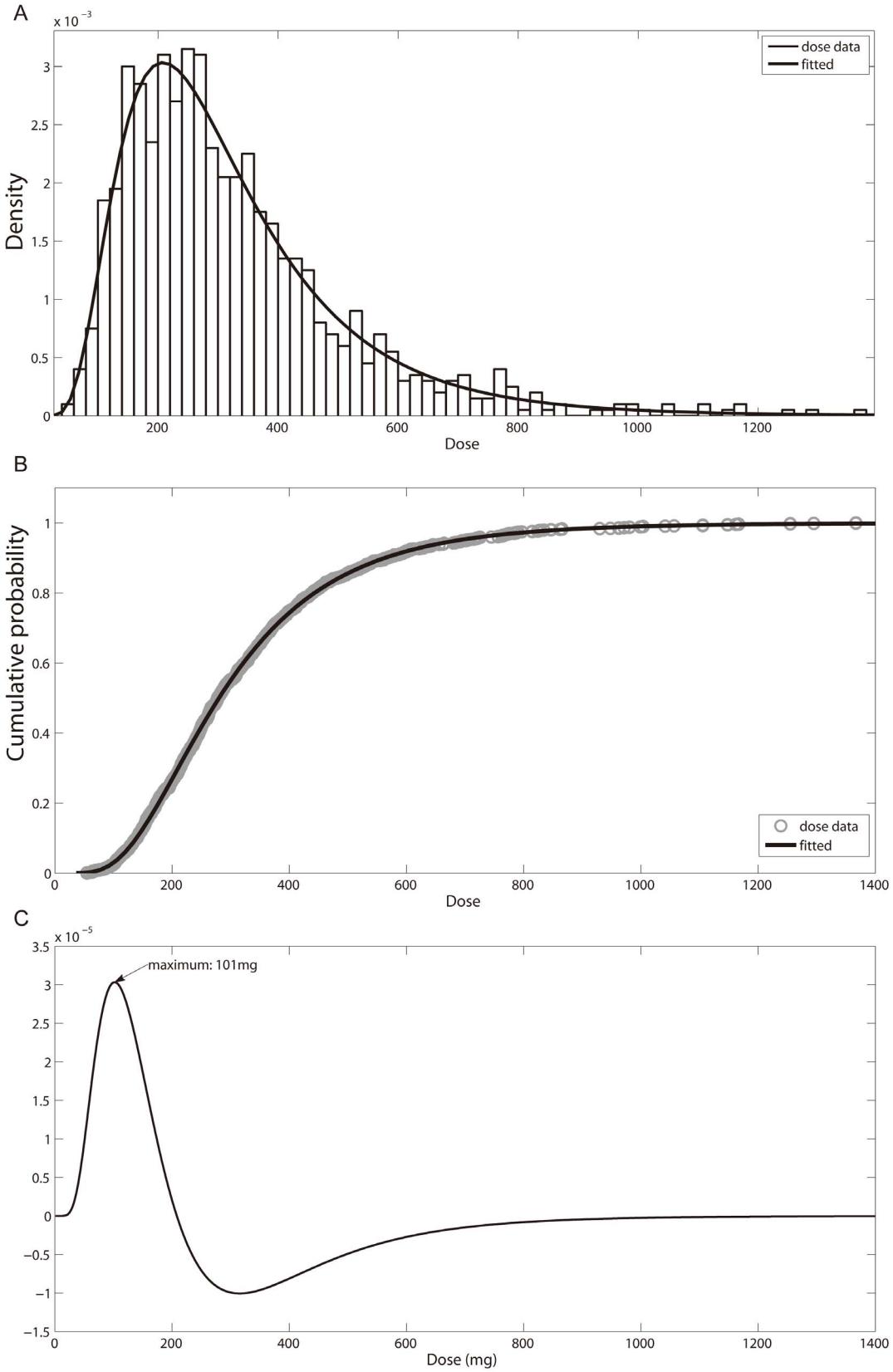
A
x 10^-3
dose data
fitted
Density
Dose
B
Cumulative probability
dose data
fitted
Dose
C
x 10^-5
maximum: 101mg
Dose (mg)

Figure 10. The simulated probability distribution of the individual dose limit in 1000 virtual elderly people. (A) The simulated dose data and fitted probability density by lognormal distribution; (B) The simulated dose data and fitted cumulative probability by log normal distribution; (C) The second derivative of the cumulative probability function and the critical value.

doi:10.1371/journal.pone.0114049.g010

related), the RAAS module (feedback related) and the electrolyte module (end point related). The 24 h urinary cortisol:cortisone ratio is a generally accepted biomarker of the inhibiton of 11β-HSD 2 and sensitive to changes in the GA level in the kidney. In the present PD model, not only the ratio but also the urinary excretion of cortisol and cortisone could be predicted and further validated by comparison with experimental data. This made the further prediction of kidney exposure to cortisol more reasonable. In addition to the 24 h urinary cortisol:cortisone ratio, serum electrolytes (potassium and sodium) and RAAS are also important indicators of GL-induced pseudoaldosteronism and are more indicative of the occurrence of adverse effects. In the present PD model, the plasma levels of angiotensin II, aldosterone, potassium and sodium were estimated and compared with the normal ranges of each indicator to predict the occurrence of adverse effects. Since there is no gold standard for GL-induced pseudoaldosteronism and since, of the various indicators of pseudoaldosteronism, serum potassium (hypokalemia) is an independent risk factor with the narrowest normal range (3.5–5 mmol/l) [48] and quite sensitive to the over-activation of MR [34, 37], we chose serum potassium as the main indicator in the simulation and prediction of the safe dose of GL.

After validation of the PKPD model, it was used to analyze the safe dose of GL. According to the SCF, a prudent dose of GL not exceeding 100 mg/day is recommended which is the LOAEL value in the most sensitive individuals. The simulation of the population mean in this scenario by the present model shows that 100 mg/day produces a less than 0.1 mmol/l decrease in the serum potassium level, which is considered safe for normal people. The screening results show that sinusoidal transport function, colonic transit time and the activity of 11β-HSD 2 are all important factors contributing to the inter-individual variability in experiencing adverse effects. In the present study, we considered the elderly as a high risk population and estimated the distribution of the individual dose limit based on data from recent studies.

In reality, describing an adverse effect should include three major factors: the dose limit, the specified population and the corresponding incidence of adverse effects. The present study provided the probability distribution of the individual dose limit in a virtual elderly population and calculated the critical value as the dose limit recommended by the present model. Interestingly, the critical value of 101 mg in our virtual elderly population was almost identical with the dose limit of 100 mg recommended by SCF. However, it must be pointed out that the SCF dose limit is an experimental value based on the clinically observed symptoms of pseudoaldosteronism while our critical value is based only on the serum potassium level. Also, the PKPD model provides the probability of increasing dose in a virtual population of 3.07% at the critical value which cannot be obtained

from clinical observations of adverse effects due to ethical concerns. This is the most important advantage of modeling and simulation compared to clinical experiments. In further clinical trials, if new factors such as drug-drug interactions or the effects of polymorphism, or other metabolites of GL are discovered to be involved in producing adverse effects, they can be introduced into the model. In addition, the model can be used to simulate scenarios which may not be included in clinical trials.

In summary, we have developed a comprehensive PBPK/PD model based on PK data and pharmacology to predict the occurrence of GL-induced pseudoaldosteronism. In this model, not only the urinary cortisol:cortisone ratio but also RAAS and serum potassium and sodium levels could be predicted. Furthermore, the present model simulated the probability distribution of the individual dose limit in a virtual population and provided the critical value of the dose limit to be recommended when GL is used as a food additive. This work would be useful to improve the safe use of GL as a food additive and drug.

Supporting Information

Appendix S1. Main equations of the PBPK model for GL and its metabolites in rat and human.
doi:10.1371/journal.pone.0114049.s001 (DOC)

Appendix S2. Main equations in the PD model for pseudoaldosteronism.
doi:10.1371/journal.pone.0114049.s002 (DOC)

Acknowledgments

The authors would like to thank Dr. John Paul Fawcett, School of Pharmacy, University of Otago for assistance in the preparation of the manuscript and for helpful discussions.

Author Contributions

Conceived and designed the experiments: JY RX XL. Performed the experiments: RX. Analyzed the data: RX JY XL. Contributed reagents/materials/analysis tools: JY. Wrote the paper: RX JY.

References

1. **Asl MN, Hosseinzadeh H** (2008) Review of pharmacological effects of Glycyrrhiza sp. and its bioactive compounds. Phytother Res 22: 709–724.
2. **Omar HR, Komarova I, El-Ghonemi M, Fathy A, Rashad R, et al.** (2012) Licorice abuse: time to send a warning message. Ther Adv Endocrinol Metab 3: 125–138.
3. **Farese RV Jr, Biglieri EG, Shackleton CH, Irony I, Gomez-Fontes R** (1991) Licorice-induced hypermineralocorticoidism. N Engl J Med 325: 1223–1227.

4. **Pippal JB, Fuller PJ** (2008) Structure-function relationships in the mineralocorticoid receptor. J Mol Endocrinol 41: 405–413.
5. **Makino T, Ohtake N, Watanabe A, Tsuchiya N, Imamura S, et al.** (2008) Down-regulation of a hepatic transporter multidrug resistance-associated protein 2 is involved in alteration of pharmacokinetics of glycyrrhizin and its metabolites in a rat model of chronic liver injury. Drug Metab Dispos 36: 1438–1443.
6. European Conmmission, Health & Consumer Protection Directorate-General, and Scientific Committee on Food. Opinion of the scientific committee on food on glycyrrhizinic acid and its ammonium salt 2003; Available: http://ec.europa.eu/food/fs/sc/scf/out186_en.pdf.
7. **Fenwick GR** (1990) Liquorice, Glycyrrhiza glabra L.—Composition, uses and analysis. Food Chemistry 38: 119–143.
8. **Ploeger BA, Meulenbelt J, DeJongh J** (2000) Physiologically based pharmacokinetic modeling of glycyrrhizic acid, a compound subject to presystemic metabolism and enterohepatic cycling. Toxicol Appl Pharmacol 162: 177–188.
9. **Ploeger B, Mensinga T, Sips A, Meulenbelt J, DeJongh J** (2000) A human physiologically-based model for glycyrrhzic acid, a compound subject to presystemic metabolism and enterohepatic cycling. Pharm Res 17: 1516–1525.
10. **Ploeger B, Mensinga T, Sips A, Deerenberg C, Meulenbelt J, et al.** (2001) A population physiologically based pharmacokinetic/pharmacodynamic model for the inhibition of 11-beta-hydroxysteroid dehydrogenase activity by glycyrrhetic acid. Toxicol Appl Pharmacol 170: 46–55.
11. **Xu R, Xiao Q, Cao Y, Yang J** (2013) Comparison of the Exposure of Glycyrrhizin and its Metabolites and the Pseudoaldosteronism after Intravenous Administration of Alpha- and Beta-glycyrrhizin in Rat. Drug Res (Stuttg) 63: 620–624.
12. **Ismair MG, Stanca C, Ha HR, Renner EL, Meier PJ, et al.** (2003) Interactions of glycyrrhizin with organic anion transporting polypeptides of rat and human liver. Hepatol Res 26: 343–347.
13. **Shimamura H, Suzuki H, Tagaya O, Horie T, Sugiyama Y** (1996) Biliary excretion of glycyrrhizin in rats: kinetic basis for multiplicity in bile canalicular transport of organic anions. Pharm Res 13: 1833–1837.
14. **Akao T, Hattori M, Kanaoka M, Yamamoto K, Namba T, et al.** (1991) Hydrolysis of glycyrrhizin to 18 beta-glycyrrhetyl monoglucuronide by lysosomal beta-D-glucuronidase of animal livers. Biochem Pharmacol 41: 1025–1029.
15. **Ishida S, Sakiya Y, Ichikawa T, Taira Z** (1992) Dose-dependent pharmacokinetics of glycyrrhizin in rats. Chem Pharm Bull (Tokyo) 40: 1917–1920.
16. **Yamamura Y, Kawakami J, Santa T, Kotaki H, Uchino K, et al.** (1992) Pharmacokinetic profile of glycyrrhizin in healthy volunteers by a new high-performance liquid chromatographic method. J Pharm Sci 81: 1042–1046.
17. **Brown RP, Delp MD, Lindstedt SL, Rhomberg LR, Beliles RP** (1997) Physiological parameter values for physiologically based pharmacokinetic models. Toxicol Ind Health 13: 407–484.
18. **Ichikawa T, Ishida S, Sakiya Y, Akada Y** (1984) High-performance liquid chromatographic determination of glycyrrhizin and glycyrrhetinic acid in biological materials. Chem Pharm Bull (Tokyo) 32: 3734–3738.
19. **Ishida S, Sakiya Y, Ichikawa T, Taira Z, Awazu S** (1990) Prediction of glycyrrhizin disposition in rat and man by a physiologically based pharmacokinetic model. Chem Pharm Bull (Tokyo) 38: 212–218.
20. **Poulin P, Theil FP** (2000) A priori prediction of tissue:plasma partition coefficients of drugs to facilitate the use of physiologically-based pharmacokinetic models in drug discovery. J Pharm Sci 89: 16–35.
21. **Poulin P, Jones RD, Jones HM, Gibson CR, Rowland M, et al.** (2011) PHRMA CPCDC initiative on predictive models of human pharmacokinetics, part 5: Prediction of plasma concentration-time profiles in human by using the physiologically-based pharmacokinetic modeling approach. J Pharm Sci.
22. **Ishida S, Sakiya Y, Taira Z** (1994) Disposition of glycyrrhizin in the perfused liver of rats. Biol Pharm Bull 17: 960–969.
23. **Wang Z, Nishioka M, Kurosaki Y, Nakayama T, Kimura T** (1995) Gastrointestinal absorption characteristics of glycyrrhizin from glycyrrhiza extract. Biol Pharm Bull 18: 1238–1241.

24. **Wang Z, Kurosaki Y, Nakayama T, Kimura T** (1994) Mechanism of gastrointestinal absorption of glycyrrhizin in rats. Biol Pharm Bull 17: 1399–1403.

25. **Parke DV, Pollock S, Williams RT** (1963) The Fate of Tritium-Labelled Beta-Glycyrrhetic Acid in the Rat. J Pharm Pharmacol 15: 500–506.

26. **Ishida S, Sakiya Y, Ichikawa T, Taira Z** (1993) Uptake of glycyrrhizin by isolated rat hepatocytes. Biol Pharm Bull 16: 293–297.

27. **Lu Y, Zhu J, Chen X, Li N, Fu F, et al.** (2009) Identification of human UDP-glucuronosyltransferase isoforms responsible for the glucuronidation of glycyrrhetinic acid. Drug Metab Pharmacokinet 24: 523–528.

28. **Austin RP, Barton P, Cockroft SL, Wenlock MC, Riley RJ** (2002) The influence of nonspecific microsomal binding on apparent intrinsic clearance, and its prediction from physicochemical properties. Drug Metab Dispos 30: 1497–1503.

29. **Kawakami J, Yamamura Y, Santa T, Kotaki H, Uchino K, et al.** (1993) Kinetic analysis of glycyrrhetic acid, an active metabolite of glycyrrhizin, in rats: role of enterohepatic circulation. J Pharm Sci 82: 301–305.

30. **Takeda S, Ishthara K, Wakui Y, Amagaya S, Maruno M, et al.** (1996) Bioavailability study of glycyrrhetic acid after oral administration of glycyrrhizin in rats; relevance to the intestinal bacterial hydrolysis. J Pharm Pharmacol 48: 902–905.

31. **Xu R, Zhang X, Yang J, Liu X, Davey AK, et al.** (2012) Effects of glycyrrhizin on biliary transport and hepatic levels of glutathione in rats. Biopharm Drug Dispos 33: 235–245.

32. **Akao T** (1997) Hydrolysis of glycyrrhetyl mono-glucuronide to glycyrrhetic acid by glycyrrhetyl mono-glucuronide beta-D-glucuronidase of Eubacterium sp. GLH. Biol Pharm Bull 20: 1245–1249.

33. **Makino T, Okajima K, Uebayashi R, Ohtake N, Inoue K, et al.** (2012) 3-Monoglucuronyl-glycyrrhretinic acid is a substrate of organic anion transporters expressed in tubular epithelial cells and plays important roles in licorice-induced pseudoaldosteronism by inhibiting 11beta-hydroxysteroid dehydrogenase 2. J Pharmacol Exp Ther 342: 297–304.

34. **MacKenzie MA, Hoefnagels WH, Jansen RW, Benraad TJ, Kloppenborg PW** (1990) The influence of glycyrrhetinic acid on plasma cortisol and cortisone in healthy young volunteers. J Clin Endocrinol Metab 70: 1637–1643.

35. **Costa A, Benedetto C, Fabris C, Giraudi GF, Testori O, et al.** (1996) Cortisol in human tissues at different stages of life. J Endocrinol Invest 19: 463–471.

36. **Ikeda N, Marumo F, Shirataka M, Sato T** (1979) A model of overall regulation of body fluids. Ann Biomed Eng 7: 135–166.

37. **Epstein MT, Espiner EA, Donald RA, Hughes H** (1977) Effect of eating liquorice on the renin-angiotensin aldosterone axis in normal subjects. Br Med J 1: 488–490.

38. **Guillaud F, Hannaert P** (2010) A computational model of the circulating renin-angiotensin system and blood pressure regulation. Acta Biotheor 58: 143–170.

39. **Williams GH** (2005) Aldosterone biosynthesis, regulation, and classical mechanism of action. Heart Fail Rev 10: 7–13.

40. **Beretta-Piccoli C, Weidmann P, Boehringer K, Link L, Bianchetti MG, et al.** (1984) Relationship between plasma aldosterone and angiotensin II before and after noradrenergic inhibition in normal subjects and patients with mild essential hypertension. J Clin Endocrinol Metab 59: 316–320.

41. **Himathongkam T, Dluhy RG, Williams GH** (1975) Potassim-aldosterone-renin interrelationships. J Clin Endocrinol Metab 41: 153–159.

42. **Nies AT, Niemi M, Burk O, Winter S, Zanger UM, et al.** (2013) Genetics is a major determinant of expression of the human hepatic uptake transporter OATP1B1, but not of OATP1B3 and OATP2B1. Genome Med 5: 1.

43. **Furihata T, Satoh T, Yamamoto N, Kobayashi K, Chiba K** (2007) Hepatocyte nuclear factor 1 alpha is a factor responsible for the interindividual variation of OATP1B1 mRNA levels in adult Japanese livers. Pharm Res 24: 2327–2332.

44. **Yamamoto T, Hatanaka M, Matsuda J, Kadoya H, Takahashi A, et al.** (2010) [Clinical characteristics of five elderly patients with severe hypokalemia induced by glycyrrhizin derivatives]. Nihon Jinzo Gakkai Shi 52: 80–85.

45. **Homma M, Ishihara M, Qian W, Kohda Y** (2006) [Effects of long term administration of Shakuyaku-kanzo-To and Shosaiko-To on serum potassium levels]. Yakugaku Zasshi 126: 973–978.

46. **Madsen JL** (1992) Effects of gender, age, and body mass index on gastrointestinal transit times. Dig Dis Sci 37: 1548–1553.

47. **Campino C, Martinez-Aguayo A, Baudrand R, Carvajal CA, Aglony M, et al.** (2013) Age-related changes in 11beta-hydroxysteroid dehydrogenase type 2 activity in normotensive subjects. Am J Hypertens 26: 481–487.

48. **Kratz A, Ferraro M, Sluss PM, Lewandrowski KB** (2004) Case records of the Massachusetts General Hospital. Weekly clinicopathological exercises. Laboratory reference values. N Engl J Med 351: 1548–1563.

49. **Ishida S, Ichikawa T, Sakiya Y** (1988) Binding of glycyrrhetinic acid to rat plasma, rat serum albumin, human serum, and human serum albumin. Chem Pharm Bull (Tokyo) 36: 440–443.

50. **Palermo M, Shackleton CH, Mantero F, Stewart PM** (1996) Urinary free cortisone and the assessment of 11 beta-hydroxysteroid dehydrogenase activity in man. Clin Endocrinol (Oxf) 45: 605–611.